Research Article Vol. 4, No. 2 / 15 February 2021 / OSA Continuum 315

Multidimensional topological strings by curved potentials: Simultaneous realization of a mobility edge and topological protection

CHUN-YAN LIN,[1] GIULIA MARCUCCI,[2,3] GANG WAN,[4] YOU-LIN CHUANG,[5] CLAUDIO CONTI,[2] AND R.-K. LEE[1,5,*]

[1]*Institute of Photonics Technologies, National Tsing Hua University, Hsinchu 300, Taiwan*
[2]*ISC-CNR and Department of Physics, University Sapienza, Rome 00185, Italy*
[3]*Department of Physics, University of Ottawa, Ontario K1N 6N5, Canada*
[4]*School of Physical Science and Technology, Soochow University, Suzhou 215006, China*
[5]*Physics Division, National Center for Theoretical Sciences, Hsinchu 30013, Taiwan*
[*]*rklee@ee.nthu.edu.tw*

Abstract: By considering a cigar-shaped trapping potential elongated in a proper curvilinear coordinate, we discover a new form of wave localization that arises from the interplay of geometry and topological protection. The potential is undulated in its shape such that local curvature introduces a geometrical potential. The curvature varying along the trap curvilinear axis encodes a topological Harper modulation. The varying geometry maps our system in a one-dimensional Andre-Aubry-Harper grating. We show that a mobility edge exists and topologically protected states arise. These states are extremely robust against disorder in the shape of the string. The results may be relevant to localization phenomena in Bose-Einstein condensates, optical fibers and waveguides, and new laser devices.

1. Introduction

Topological concepts pervade modern physics, including photonics, Bose-Einstein condensation (BEC), condensed matter physics, and high-energy physics, with the illustrations on the difference between bulk and boundary, chiral symmetry, adiabatic equivalence, topological invariants, and bulk–boundary correspondence. Topology enriches physical systems with non-trivial symmetries that protect specific features with respect to disorder, as the energy eigenvalues of localized states. In addition, properly designed topological systems may link to analog additional dimensions in a way such that one can mimic multidimensional physics in the four-dimensional world [1–3]. By taking the quasi-crystal structure as a platform, Andre-Aubry-Harper (AAH) model has provided a simple one-dimensional model with the parameter being synthetic dimension [4]. Through the analogy in single-particle Hamiltonian, topologically non-trivial modes can also be observed in various platforms such as waveguide arrays [5,6], cavity arrays [7], cold atom lattices [8], and split-ring resonator (SRR) arrays [9–12], with a periodically setting on the confined potentials. Specifically, topological edge states, may be induced at the interface between media with different topological features as Chern number. Topological edge states are recently demonstrated to be very useful for a new generation of lasers, and attracted considerable attention [13–18].

In parallel to topology, geometrical features may also bring forth different forms of localization, if a flat system is curved by a continuous deformation [19–24]. The local curvature creates an effective trapping potential, the so-called geometrical potential. For example, the interplay of disordered induced localization and geometry has been analyzed in Ref. [25]. Also curvature induced localization has recently been exploited to induce states at maximal curvature points in vertical cavity lasers [26], as well as to speckle reduction in imaging projection [27]. However, this effect is influenced by unwanted and random deformations.

#413213 https://doi.org/10.1364/OSAC.413213
Journal © 2021 Received 23 Oct 2020; accepted 23 Dec 2020; published 25 Jan 2021

OSA CONTINUUM

May we use topological protection to stabilize localized states due to local curvature? The connection and the interplay between the two forms of localization are unexplored. In this paper we show that by combining geometrical and topological potentials, one obtains new kinds of localized states. We identify specific - open or closed - "topological strings," such that the localized states of the curvature profile are robust with respect to the deformation. In addition, we know that some of the most important theoretical models of modern physics are related to two-dimensional strings embedded in multidimensional space. One can argue that if one can realize these kinds of systems in the laboratory, then it is possible to study five-dimensional strings. Here, we show that a workable strategy is given by our topological strings. Their excitations, as localized states, may represent analogues of fundamental physical particles [28]. Through the analogy in single-particle Hamiltonian, various systems are suitable for the experimental realization of these topological strings, such as BEC with an elongated potential, curved optical waveguides and lasers, and polymer physics.

The rest of the paper is structured as follows. In Sec. 2, we outline the derivation of the reduced 1D equation in the curvilinear coordinate, starting from the 3D Schrödinger equation. Then, in Sec. 3, the methodology to construct topological string by a sequence of parabolas is illustrated. The equivalence between our topological string and AAH model is demonstrated in Sec. 4, with examples for the localized/delocalized states and their inverse participation ratio (IPR) index as a quantitative figure of merit. The paper is summarized in Sec. 5.

2. Reduced 1D equation in the curvilinear coordinate

As illustrated in Fig. 1, what we adopt as a reference model is the three-dimensional (3D) Schrödinger equation, i.e.,

$$i\,\Psi_t = -\nabla^2\Psi + V_{3D}\Psi. \tag{1}$$

The concepts described in the following may also apply to the other systems, as lasers, optical fibers and waveguides described in the paraxial wave equations. Here, we consider a curved potential in the 3D space [Fig. 1(a)], i.e., $V_{3D} = V_1(q_1) + V_\perp(q_2, q_3)$, where $q_1 \equiv q$ is the longitudinal coordinate along the arc, and q_2, q_3 are the transverse coordinates [19,24]. In Eq. (1), $V_\perp$ determines the transverse confinement along an arbitrary curve, whose curvilinear coordinate is given by q. Specifically, we consider parabolic potentials in the form: $V_\perp = w(q_2^2 + q_3^2)$, $V_1(q_1) = w_1\, q_1^2$, with $w \gg w_1$. Being $\lambda^2 = w/w_1$, the 1D reduction holds true as $\lambda^2 \to \infty$ [19]. Then, by separation of variables, one can assume the solution in the form: $\Psi(q_1, q_2, q_3, t) = l_\perp \psi_\perp(q_2, q_3)\psi(q)\exp(-i\,E_\perp t)$, with $\int |\psi_\perp(q_2, q_3)|^2\, dq_2 dq_3 = 1$ and $E_\perp$ the transverse part of the eigenvalue. The transverse localization length is $l_\perp^{-2} = \int |\psi_\perp(q_2, q_3)|^4\, dq_2 dq_3$, along with the normalization condition $\int |\psi(q)|^2\, dq = N l_\perp^{-2} \equiv P$. For the parabolic potential above, the resulting reduced 1D Schrödinger equation has an effective 1D potential,

$$i\,\partial_t\psi = -\partial_q^2\psi + V(q)\psi, \tag{2}$$

which gives a geometrical potential $V = V_1 + V_G$. Explicitly, one can denote the parabola in a 2D plane, as illustrated in Fig. 2, by setting $Y = k\,X^2$. Please note that our reference coordinate is X-axis. Then, the corresponding maximum curvature is $2\,k = 1/R$, with R denoting the radius of curvature. In terms of the local curvature $K(q)$, the corresponding geometrical potential V_G has the form

$$V_G(q) = -\frac{K(q)^2}{4}. \tag{3}$$

Now, for a parabola, the local curvature can be derived as

$$K(q)^2 = |\frac{d\hat{t}}{dX}|^2\,|\frac{dX}{dq}|^2 = \frac{4k^2}{[1 + 4\,k^2\,X(q)^2]^3}. \tag{4}$$

OSA CONTINUUM

Here, $\hat{t}$ denotes the normalized tangent vector along the curvilinear coordinate q. The implicit function $X(q)$ is given by the inverse of $4\,k\,q = 2\,k\,X\sqrt{1+4\,k^2\,X^2} + \sinh^{-1}(2\,k\,X)$.

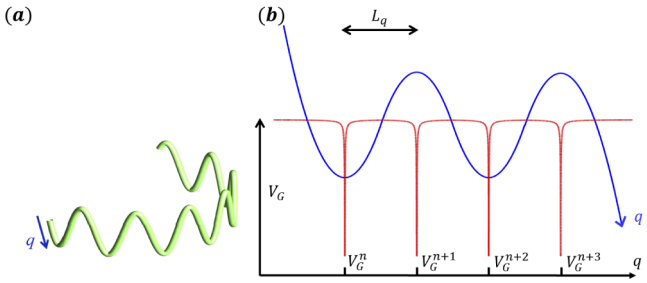

Fig. 1. (a) Sketch of a topological string made by a 3D trapping potential; and (b) in the curvilinear coordinate q, we show such a topological string formed by four segments of parabolas in Blue-color with the corresponding potential V_G in Red-color. Here, L_q denotes the distance between two parabolic segments, with the corresponding local minimum value in each segment indicated as V_G^{n+i}, $i = 0, 1, 2, 3$.

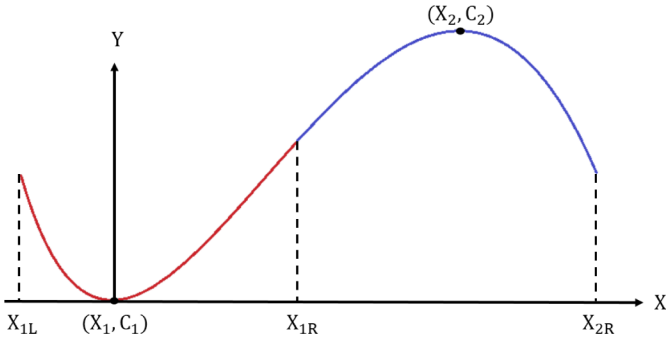

Fig. 2. The illustration to construct a topological string. Here, we take two parabolic segments plotted in Red- and Blue-colors as an example. The the front (left), end (right) points labelled in X_{1L}, X_{1R}, X_{2R} denote the projections of the segments onto our reference coordinate X-axis; while (X_1, C_1) and (X_2, C_2) denote the extremum (minimum and maximum) of the local curvature in each parabola.

With such a reduction to the curvilinear coordinate q, in Fig. 1(b), we illustrate an example showing the local potential $V_G(q)$ for a four parabolic segments string in Blue-color. As one can see for the corresponding potential V_G in Red-color, now, one can modulate the local minimum value in each segment by varying the curvature in each parabola. In the following, we consider a modulate path characterized by a repetition of parabolas merged with straight line. By using Eqs. (2–3), we aim at determining the path that realize a Harper modulation. The topological strings are 3D objects that are modulated in one dimension by a Harper potential, which is known to simulate additional synthetic coordinates. By including also the time evolution, the system simulates a string in a five dimensional space.

3. Topological string constructed by parabolas

Our topological potential is composited by a sequence of parabolas. To merge each segment together, we fix the distance between two parabolic segments as a constant, denoted as L_q in Fig. 1(b). Adopting a Cartesian set (X, Y), as illustrated in Fig. 2, each branch of the parabolas

OSA CONTINUUM

has extremum (maximum or minimum) in (X_j, C_j), with the local curvature is k_j. Explicitly, for each branch of the parabola we have

$$Y = \pm k_n (X - X_n)^2 + C_n, \tag{5}$$

with the offset denoted as C_n. In Eq. (5), the plus sign is applied when the parabola opens up; while the minus sign is applied when the parabola opens down. As shown in Eq. (3), the corresponding maximum of the potential is related to the curvature $V_G^n = -k_n^2$. By merging the different branches and imposing the continuity profile, we find that one can build a Harper modulation with a constant distance L_q between the maximum curvature points that are located at positions $X = X_n$ and $Y = C_n$ with the curvature coefficient k^n, with $n = 1, 2, \ldots, N$.

To construct the topological strings, for each parabolic segments, in addition to the local curvature k_n and the given distance L_q, we also have two free parameters X_n and C_n, corresponding to the center of the parabola and its offset. Here, we fix the distance between two segment as a constant, i.e., $L_q = 6$, but vary the offset of the adjacent parabola to mimic the Harper modulation. As for the curvature, the adjacent parabolas have the different sign, in order to have a smooth connection. As illustrated in Fig. 2, to have a continuous derivative in the connected segment, we have

$$Y_n'(X_{nR}) = Y_{n+1}'(X_{nR} = X_{(n+1)L}),$$

or equivalently,

$$X_{n+1} = [(k_n + k_{n+1})X_{nR} - k_n X_n]/k_{n+1}.$$

Then, for a fix value in L_q, we have $L_q = q_{nR} + q_{(n+1)L}$. For the offset, we have

$$C_{n+1} = C_n + k_n (X_{nR} - X_n)^2 \pm k_{n+1} (X_{nR} - X_{n+1})^2,$$

where we set the plus sign for the odd number in segments; and minus sign for the even number.

4. Equivalence between the topological string and AAH model

To have the corresponding Harper modulation, by fixing the period with the distance between two branches L_q, we calculate the potential peak $V_G(nL_q) = V_0 + V_1 \cos(2\pi\alpha n + \delta)$ for each portion of the parabola, in order to have a set of localized potentials. In the tight binding approximation (V_0 is omitted hereafter without loss of generality), we have

$$t\,(\psi_{n+1} + \psi_{n-1}) + V_1 \cos(2\pi\alpha n + \delta)\psi_n = E_n\,\psi_n. \tag{6}$$

In Eq. (6), the hopping constant is denoted by t and the corresponding energy eigenvalue is E_n. In the AAH model, V_1 is the strength of the modulation, α is modulation frequency, and the phase term δ gives the synthetic dimension [4]. Compared to the well-known AAH model characterized by its hopping constant t and the Harper modulation V_1, here, we describe our topological string by the length L_q between two segments, and local curvature k_n.

It is known that in AAH model there exists a critical value for the ratio between Harper modulation and the hopping constant, V_1/t, which equivalently corresponds to $L_q \times k_n$ in our topological string. When $V_1/t>2$, localized states are supported; for $V_1/t<2$ all the modes are delocalized. The transition from delocalized to localized modes is expected when the modulation frequency α is an irrational number, for example $\alpha = (1 + \sqrt{5})/2$. This case is referred to as the so called incommensurate Harper model; it is specifically relevant as a one-dimensional model with a mobility edge in analogy with the Anderson model.

As illustrated in Fig. 3, the band-diagrams for the AAH model in Eq. (6) support mobility edge states (red color), independently of V_1/t. Instead of Brillouin zone defined in reciprocal space, here, the phase term δ defined in the AAH model, see Eq. (6), provides the synthetic dimension

OSA CONTINUUM

for the band-diagram. For the mobility edge states, the existence region in the band-gap becomes narrower when our system only supports localized states, see Fig. 3(a) for $V_1/t = 3$. Nevertheless, when delocalized states are supported, see Fig. 3(b) for $V_1/t = 1$, the existence region in the band-gap becomes broader.

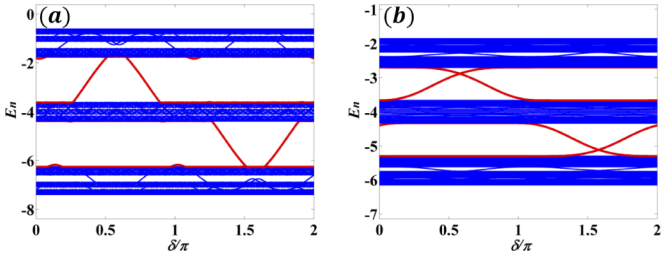

Fig. 3. Band diagrams for the AAH model in Eq. (6), for the ratio between Harper modulation and the hopping constant, V_1/t, larger than the critical value (a) $V_1/t = 3$ with all states localized; and smaller than the critical value (b) V_1/t with delocalized states. Red-curves denotes the mobility edge states. Here, parameters used are $V_0 = -4$ and $\alpha = (1+\sqrt{5})/2$, which gives the critical value $V_1/t = 2$.

4.1. Examples

To test that our geometrical potential mimics the Harper model in an equivalent way, we study the modes for $N = 20$ segments. Then, we calculate the eigenstates of this effective potential along the curvilinear coordinate by following the methodology illustrated in Sec. 3. A series of localized states and also delocalized functions are found for a different setting on the parameter $k_n \times L_q$. A key challenge is showing if the topological and geometrical potential $V(q)$ inherit the features of the discrete Harper modulation. In terms of the string parameters, the critical value for the localization-delocalization transition is defined by the product of the maximum local curvature and the length of string, i.e., $k_m \times L_q$. By numerical simulations, we have $k_m \times L_q \approx 7.0$.

As an illustration for some representative cases, in Figs. 4 and 5, we show the field profiles (in Blue-color) and the corresponding geometrical potential (in Red-color) given by a series of localized traps with varying amplitudes V_G. First of all, in Fig. 4(a-b), we illustrate the localized state supported in AAH model in Blue-colors, with the corresponding disorder potential V_G, based on the band-diagram illustrated in Fig. 3. In addition to these localized states, in Fig. 4(c-d), one can see the supported mobility edge states and the corresponding topological string in 3D space. With a proper setting on the curvatures in the string, our topological strings indeed support non-trivial mobility edge modes in the front (or end) branch.

Instead, when we choose $k_m \times L_q = 6.61 < 7.0$, we show the delocalized state supported in our topological string in Fig. 5(a-b). Since the value $k_m \times L_q$ is smaller than the critical value, our topological string does not support localized states as expected. Nevertheless, mobility edge states can still be found, as shown in Fig. 5(c-d), which demonstrates that these mobility edge states are robust with respect to disorder in shape of the string.

4.2. Inverse participation ratio (IPR)

Our *topological string* works effectively as the AAH model. By mapping our system into the discrete AAH model, we can estimate the corresponding Harper modulation and the hopping constant. In order to give a quantitative figure of merit to verify localization-delocalization transition in the topological strings, we also calculate the inverse participation ratio (IPR) index

OSA CONTINUUM

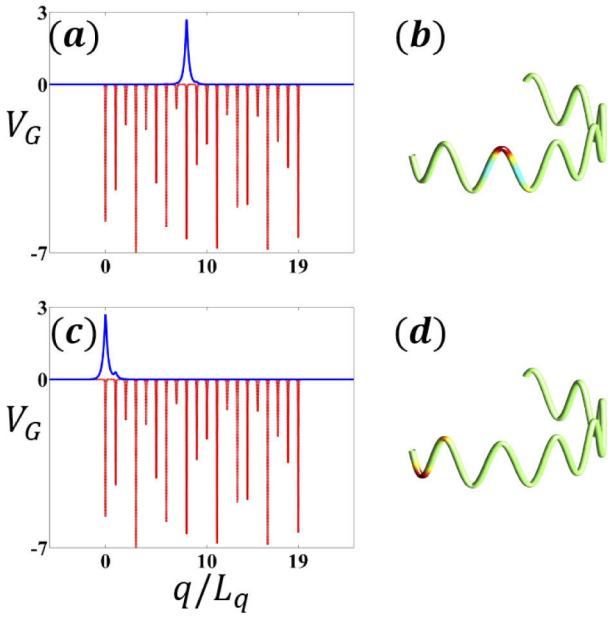

Fig. 4. (a) Localized states in the topological string: Blue-curve gives the field profile; while Red-curve reveals the corresponding disordered potential V_G; (b) the corresponding topological string in 3D space. (c) Mobility edge state and (d) the corresponding topological string in 3D space. Parameters: $V_0 = -4$, $V_1 = 3.0$, $L_q = 6$ ($k_m \times L_q = 15.87 > 7.0$), and $\delta = 0.221$.

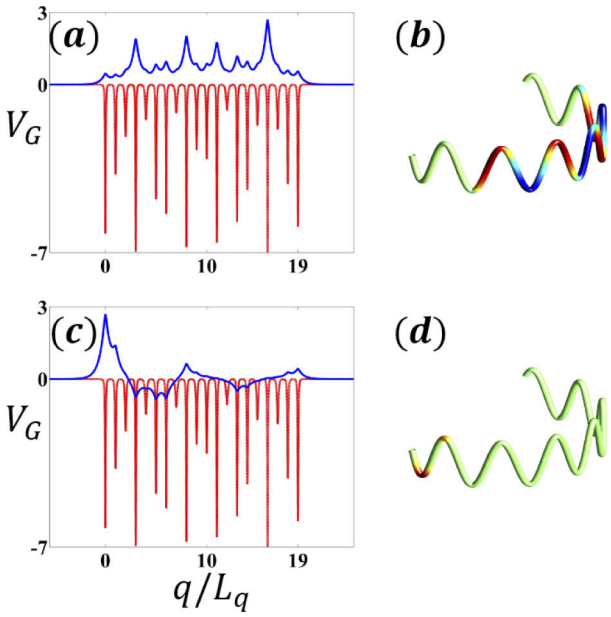

Fig. 5. (a) Delocalized states in the topological string: Blue-curve gives the field profile; while Red-curve reveals the disordered potential V_G; (b) the corresponding topological string in 3D space. (c) Mobility edge states and (d) the corresponding topological string in 3D space. Parameters: $V_0 = -4$, $V_1 = 3.0$, $L_q = 2.5$ ($k_m \times L_q = 6.61 < 7.0$), and $\delta = 0$.

OSA CONTINUUM

by defining [29],

$$\mathrm{IPR} \equiv \frac{\sum_{i=1}^{N} |\psi_i|^4}{(\sum_{i=1}^{N} |\psi_i|^2)^2}, \tag{7}$$

where N being the number of all the lattice sites. It is known that IPR index represents a measure of the number of sites contributing to a given state. The clear distinction of IPR index indicates the characteristic features of the AAH model, providing a criterion to distinguish the extended (delocalized) states from the localized ones. In Fig. 6, we show the IPR index for all the supported modes, for a different setting on the product of the maximum local curvature and the length of string, i.e., $k_m \times L_q$. Clearly, one can see that there exists a transition in IPR index at $k_m \times L_q \approx 7.0$, for the description maximum local curvature and distance between two segments of a string. Again, such a transition between localized and delocalized states verifies that our proposed topological strings can server as the platform to realize the AAH model to embed nontrivial topological protection.

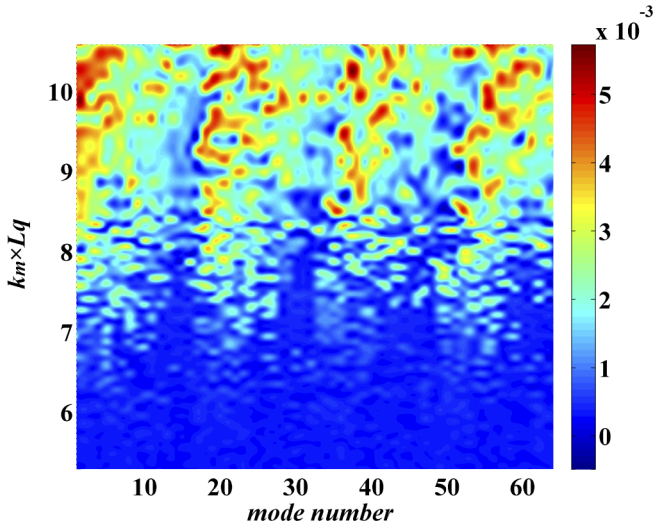

Fig. 6. The inverse participation ratio (IPR) index for all the supported modes, as a function of the product of the maximum local curvature and the length of string, i.e., $k_m \times L_q$. One can see that there exists a transition in IPR index at $k_m \times L_q \approx 7.0$.

5. Conclusion

In conclusion, by combining two different concepts, *geometrical string* and *topological protection* together, we have predicted novel localized states in string-like trapping potential with topological modulation. Curvature and topological protection commit together to support an entire new class of localized states, which are robust with respect to fluctuations of system parameters and string geometry. By combing the local curvature and global synthetic dimension together, we have introduced for the first time this class of states, which are expected to sustain novel and unexpected physical properties. In particular, with the reduced 1D equation in the curvilinear coordinate, we provide the methodology to construct topological string by a sequence of parabolas, which is equivalent to the Andre-Aubry-Harper (AAH) model. Examples are illustrated for the localized/delocalized states and their inverse participation ratio (IPR) index as a quantitative figure of merit. The proposed *topological strings* in this work provide an alternative solution to overcome the difficulties in manipulating the complex potentials. For the possible experimental realization, one can easily fabricate curves in 2D surface with an arbitrary curvature. For examples, in Ref. [26], we have experimentally demonstrated such a wave localization due to

OSA CONTINUUM

the confinement from the curvature in vertical cavity surface emitting lasers (VCSELs). With a proper setting as we illustrated in this work, it is expected to realize such *topological strings* in a similar platform. It is remarkable that using topological strings one can experimentally test the resonances and features of excitations in simulated multidimensional spaces, which can open the way to fundamental studies of string theory and related fields.

Funding. H2020 PhoQus (820392); H2020 QuantERA QUOMPLEX (731473); Ministry of Science and Technology, Taiwan (105-2628-M-007-003-MY4, 109-2112-M-007-019-MY3); CNR-MOST cooperation.

Disclosures. The authors declare no conflicts of interest.

References

1. Y. E. Kraus, Z. Ringel, and O. Zilberberg, "Four-Dimensional Quantum Hall Effect in a Two-Dimensional Quasicrystal," Phys. Rev. Lett. **111**(22), 226401 (2013).
2. M. Lohse, C. Schweizer, H. M. Price, O. Zilberberg, and I. Bloch, "Exploring 4D quantum Hall physics with a 2D topological charge pump," Nature **553**(7686), 55–58 (2018).
3. O. Zilberberg, S. Huang, J. Guglielmon, M. Wang, K. P. Chen, Y. E. Kraus, and M. C. Rechtsman, "Photonic topological boundary pumping as a probe of 4D quantum Hall physics," Nature **553**(7686), 59–62 (2018).
4. Y. E. Kraus, Y. Lahini, Z. Ringel, M. Verbin, and O. Zilberberg, "Topological States and Adiabatic Pumping in Quasicrystals," Phys. Rev. Lett. **109**(10), 106402 (2012).
5. A. B. Khanikaev, S. H. Mousavi, W.-K. Tse, M. Kargarian, A. H. MacDonald, and G. Shvets, "Photonic topological insulators," Nat. Mater. **12**(3), 233–239 (2013).
6. L. Lu, J. D. Joannopoulos, and M. Soljacic, "Topological photonics," Nat. Photonics **8**(11), 821–829 (2014).
7. X.-W. Luo, X. Zhou, C.-F. Li, J.-S. Xu, G.-C. Guo, and Z.-W. Zhou, "Quantum simulation of 2D topological physics in a 1D array of optical cavities," Nat. Commun. **6**(1), 7704 (2015).
8. N. Goldman, J. Dalibard, A. Dauphin, F. Gerbier, M. Lewenstein, P. Zoller, and I. B. Spielman, "Direct imaging of topological edge states in cold-atom systems," Proc. Natl. Acad. Sci. U. S. A. **110**(17), 6736–6741 (2013).
9. Z. Guo, H. Jiang, Y. Sun, Y. Li, and H. Chen, "Asymmetric topological edge states in a quasiperiodic Harper chain composed of split-ring resonators," Opt. Lett. **43**(20), 5142 (2018).
10. J. Jiang, Z. Guo, Y. Ding, Y. Sun, Y. Li, H. Jiang, and H. Chen, "Experimental demonstration of the robust edge states in a split-ring-resonator chain," Opt. Express **26**(10), 12891 (2018).
11. J. Jiang, J. Ren, Z. Guo, W. Zhu, Y. Long, H. Jiang, and H. Chen, "Seeing topological winding number and band inversion in photonic dimer chain of split-ring resonators," Phys. Rev. B **101**(16), 165427 (2020).
12. J. Song, F. Yang, Z. Guo, Y. Chen, H. Jiang, Y. Li, and H. Chen, "One-dimensional topological quasiperiodic chain for directional wireless power transfer," arXiv: 2008.10352 (2020).
13. L. Pilozzi and C. Conti, "Topological lasing in resonant photonic structures," Phys. Rev. B **93**(19), 195317 (2016).
14. P. St-Jean, V. Goblot, E. Galopin, A. Lematre, T. Ozawa, L. Le Gratiet, I. Sagnes, J. Bloch, and A. Amo, "Lasing in topological edge states of a one-dimensional lattice," Nat. Photonics **11**(10), 651–656 (2017).
15. G. Harari, M. A. Bandres, Y. Lumer, M. C. Rechtsman, Y. D. Chong, M. Khajavikhan, D. N. Christodoulides, and M. Segev, "Topological insulator laser: Theory," Science **359**(6381), eaar4003 (2018).
16. M. A. Bandres, S. Wittek, G. Harari, M. Parto, J. Ren, M. Segev, D. N. Christodoulides, and M. Khajavikhan, "Topological insulator laser: Experiments," Science **359**(6381), eaar4005 (2018).
17. B. Bahari, A. Ndao, F. Vallini, A. E. Amili, Y. Fainman, and B. Kante, "Nonreciprocal lasing in topological cavities of arbitrary geometries," Science **358**(6363), 636–640 (2017).
18. L. Pilozzi and C. Conti, "Topological cascade laser for frequency comb generation in *PT*-symmetric structures," Opt. Lett. **42**(24), 5174 (2017).
19. R. C. T. da Costa, "Quantum mechanics of a constrained particle," Phys. Rev. A **23**(4), 1982–1987 (1981).
20. S. Batz and U. Peschel, "Linear and nonlinear optics in curved space," Phys. Rev. A **78**(4), 043821 (2008).
21. S. Batz and U. Peschel, "Solitons in curved space of constant curvature," Phys. Rev. A **81**(5), 053806 (2010).
22. V. H. Schultheiss, S. Batz, A. Szameit, F. Dreisow, S. Nolte, A. Tnnermann, S. Longhi, and U. Peschel, "Optics in Curved Space," Phys. Rev. Lett. **105**(14), 143901 (2010).
23. C. P. Jisha, Y. Y. Lin, T. D. Lee, and R.-K. Lee, "Crescent Waves in Optical Cavities," Phys. Rev. Lett. **107**(18), 183902 (2011).
24. C. Conti, "Localization and shock waves in curved manifolds," Sci. Bull. **61**(7), 570–575 (2016).
25. C. Conti, "Linear and Nonlianear Anderson Localization in a Curved Potential," Chin. Phys. Lett. **31**(3), 030501 (2014).
26. K.-B. Hong, C.-Y. Lin, T.-C. Chang, W.-H. Liang, Y.-Y. Lai, C.-M. Wu, Y.-L. Chuang, T.-C. Lu, C. Conti, and R.-K. Lee, "Lasing on nonlinear localized waves in curved geometry," Opt. Express **25**(23), 29068 (2017).
27. Y.-C. Wang, H. Li, Y.-H. Hong, K.-B. Hong, F.-C. Chen, C.-H. Hsu, R.-K. Lee, C. Conti, T. S. Kao, and T.-C. Lu, "Flexible Organometal-Halide Perovskite Lasers for Speckle Reduction in Imaging Projection," ACS Nano **13**(5), 5421–5429 (2019).
28. J. Polchinski, *String Theory*, (Cambridge University Press, 1998).
29. B. Kramer and A. MacKinnon, "Localization: theory and experiment," Rep. Prog. Phys. **56**(12), 1469–1564 (1993).